Energy
Volume 166 Issue EN4

Sinking failure of scour protection at wind turbine foundation
Sumer and Nielsen

ice | proceedings

Proceedings of the Institution of Civil Engineers
Energy 166 November 2013 Issue EN4
Pages 170–188 http://dx.doi.org/10.1680/ener.12.00006
Paper 1200006
Received 29/05/2012 Accepted 22/11/2012

Keywords: coastal engineering/granular materials/offshore engineering

ice Institution of Civil Engineers
publishing

Sinking failure of scour protection at wind turbine foundation

1 B. Mutlu Sumer PhD
Professor, Technical University of Denmark, DTU Mekanik, Section for Fluid Mechanics, Coastal and Maritime Engineering, Lyngby, Denmark

2 Anders W. Nielsen PhD
Former PhD student, Technical University of Denmark, DTU Mekanik, Section for Fluid Mechanics, Coastal and Maritime Engineering, Lyngby, Denmark; currently Hydraulic Research Engineer, DHI, Hørsholm, Denmark

This paper summarises the results of an experimental study on scour protection around offshore wind turbine foundations, with special emphasis on the sinking failure of the scour protection work in Horns Rev 1 offshore wind farm (Denmark). The paper reviews previous results obtained by the author (AN), and is organised as follows. Section 2 addresses flow around a pile with a scour protection. Section 3 looks at the initiation of sand motion beneath scour protection. Section 4 discusses sediment motion beneath scour protection and resulting sinking. Section 5 investigates the Horns Rev 1 case. A brief account is also given of filter criteria and their application to the Horns Rev 1 case, whereby the present results and the filter criteria results are linked.

Notation

D, D_p	pile diameter
D_b	grain size of bed sediment
D_c	cover-stone size
D_f	filter-stone size
e	sinking of scour protection
e_{max}	maximum sinking of scour protection
g	acceleration due to gravity
h	water depth
I	hydraulic gradient in horizontal direction
I_{cr}	critical value of I, corresponding to initiation of sediment motion beneath filter layer
KC	Keulegan–Carpenter number, Equation 2
k	turbulent kinetic energy, $k = \frac{1}{2}(\overline{u'}^2 + \overline{v'}^2 + \overline{w'}^2)$
N_c	number of cover layers
N_f	number of filter layers
n_f	porosity of filter material
p	pressure
Re_g	grain Reynolds number based on approach velocity, $Re_g = U_\infty D_b/\nu$
s	specific gravity of sand grains
T	wave period
t_c	thickness of cover layer
t_f	thickness of filter layer
U_∞, U_c	approach current velocity
U_m	maximum value of orbital velocity of water particles at bed
u	stream-wise velocity
u', v', w'	fluctuating components of stream-wise, transverse and vertical components of velocity, respectively
x, y, z	coordinate system; see Figure 3 for definition sketch
ν	kinematic viscosity of water
Ω	sediment mobility defined by Equation 4
Ω_{cr}	critical value of Ω, corresponding to the initiation of sediment motion beneath filter layer

1. Introduction

During the past decade, more and more wind farms have been erected offshore. An ever-increasing number of offshore wind farms (OWFs) will be added to the already existing farms, because offshore wind energy has proven to be one of the key elements in the future renewable energy supply in Northern Europe. Many of these new OWFs will be placed in harsh environments and in order to reduce the costs without compromising the safety it is important to have a detailed understanding of the entire structure, including scour and scour protection around the foundations.

Although foundations of offshore wind turbines (OWTs) with no scour protection are considered to be a viable option

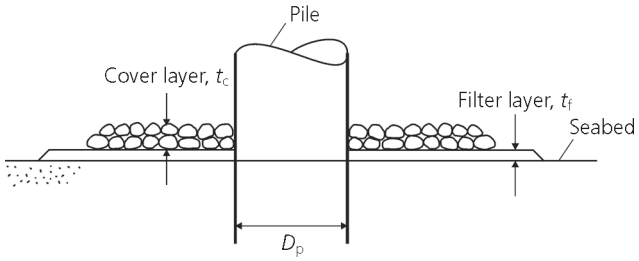

Figure 1. Definition sketch. Scour protection around foundation of offshore wind turbine

(Wittrup, 2012), a large percentage of OWT foundations are almost invariably designed to have scour protection. Rock/stone dumping is one of the methods widely used for scour protection, in which a stone cover is installed around the pile (with or without a filter layer between the seabed and the stone layer), extending over an area of three to four times the pile diameter, Figure 1.

As a consequence of the lessons learned from the first OWFs, a substantial amount of research on scour and scour protection has accumulated in recent years. Several studies have reported seabed measurements from the installed OWFs, see Hansen *et al.* (2007), Raaijmakers *et al.* (2007) and Whitehouse *et al.* (2011a, 2011b). The first two comprise data from specific wind farms (Horns Rev 1 and Egmond aan Zee, respectively). Whitehouse *et al.* (2011a) compiled data from several farms, with and without scour protection, whereas Whitehouse *et al.* (2011b) provide a review of the experience with gravity-based foundations, both prototype and model scale. Other studies have focused on prediction of the scour development, including Nielsen and Hansen (2007), Raaijmakers and Rudolph (2008a, 2008b), Harris *et al.* (2010), Nielsen *et al.* (2012) and Sumer *et al.* (2013) among others. A third group of studies have reported results from physical model tests with scour protections around the monopile foundations: Chiew (1995, 2002) and Chiew and Lim (2000) studied the stability of scour protection under current conditions, whereas de Vos *et al.* (2011, 2012) studied the stability of scour protections around a monopile under offshore conditions.

One of the first larger OWFs is the Horns Rev I installed at relatively shallow water (6·5–13 m) about 14 km off the Danish west coast in the North Sea, consisting of 80 OWTs, supported by 4·2 m diameter monopiles. This area is exposed to tidal currents and large waves from the North Sea. The wind farm was installed in the summer of 2002. A control survey in 2005 showed that the scour protections adjacent to the monopiles sank up to 1·5 m, another important failure mode of scour protection different from that studied by Chiew (1995, 2002), Chiew and Lim (2000) and de Vos *et al.* (2011, 2012). The damaged protection work has been subsequently repaired, and no significant sinking has been reported after the repair. An example of the survey results can be seen in Figure 2. Hansen *et al.* (2007) report that the 50-year-return-period tidal current velocity is 0·88 m/s. The same authors also report that the following set of wave parameters represents a typical storm situation at this locality: significant wave height, $H = 3{\cdot}5$ m; peak wave period, $T = 10$ s; and water depth, $h = 10$ m. Important features of the scour protection as well as the sand size at Horns Rev 1 are given later in Tables 3 and 6, while Figure 2 illustrates the plan view dimensions.

The above-mentioned incident prompted the present research, with the focus on obtaining an understanding of the mechanisms governing the sinking of scour protection of OWT foundations. The present research, a PhD project (Nielsen, 2011), is one of the research projects undertaken as part of the programme 'Seabed and wind farm interaction' (http://sbwi.dhigroup.com/), a 4-year (2008–2012) research programme financed by Danish Strategic Research (DSF), and coordinated by the first author.

The present paper essentially provides a review of Nielsen (2011) (also reported in Nielsen *et al.*, 2011), highlighting the key results. The paper further includes a detailed comparison between the results of Nielsen (2011) and the observed sinking at Horns Rev I OWF, and often-used design criteria for scour protections (de Graauw *et al.*, 1984).

2. Flow around a pile with scour protection

Observations show (Nielsen, 2011; Nielsen *et al.*, 2011) that when a pile with a scour protection at the bottom is placed on a bed, three major changes will occur, as follows.

(*a*) A horseshoe vortex will be formed in front of the pile, which penetrates into the scour protection (Figure 3); an accompanying, small horseshoe vortex also will be formed in front of the scour protection, as sketched in Figure 3.
(*b*) A lee-wake vortex flow will be formed behind the pile (Figure 3).
(*c*) The flow will contract in plan view at the sides of the pile.

Each flow feature will now be considered individually.

2.1 Horseshoe vortex flow

The horseshoe vortex, the key element in scour around piles, is caused by the adverse pressure gradient owing to the presence of the pile (Sumer and Fredsøe, 2002). Flow visualisation and flow measurements (using laser doppler anemometry (LDA)) made inside the scour protection (including several multi-layer cases) in Nielsen (2011; also reported in Nielsen *et al.*, 2011) indicate the flow picture, as illustrated in Figure 4.

Figure 4(a) illustrates a two-layer scour protection where the horseshoe vortex penetrates across the entire thickness of the

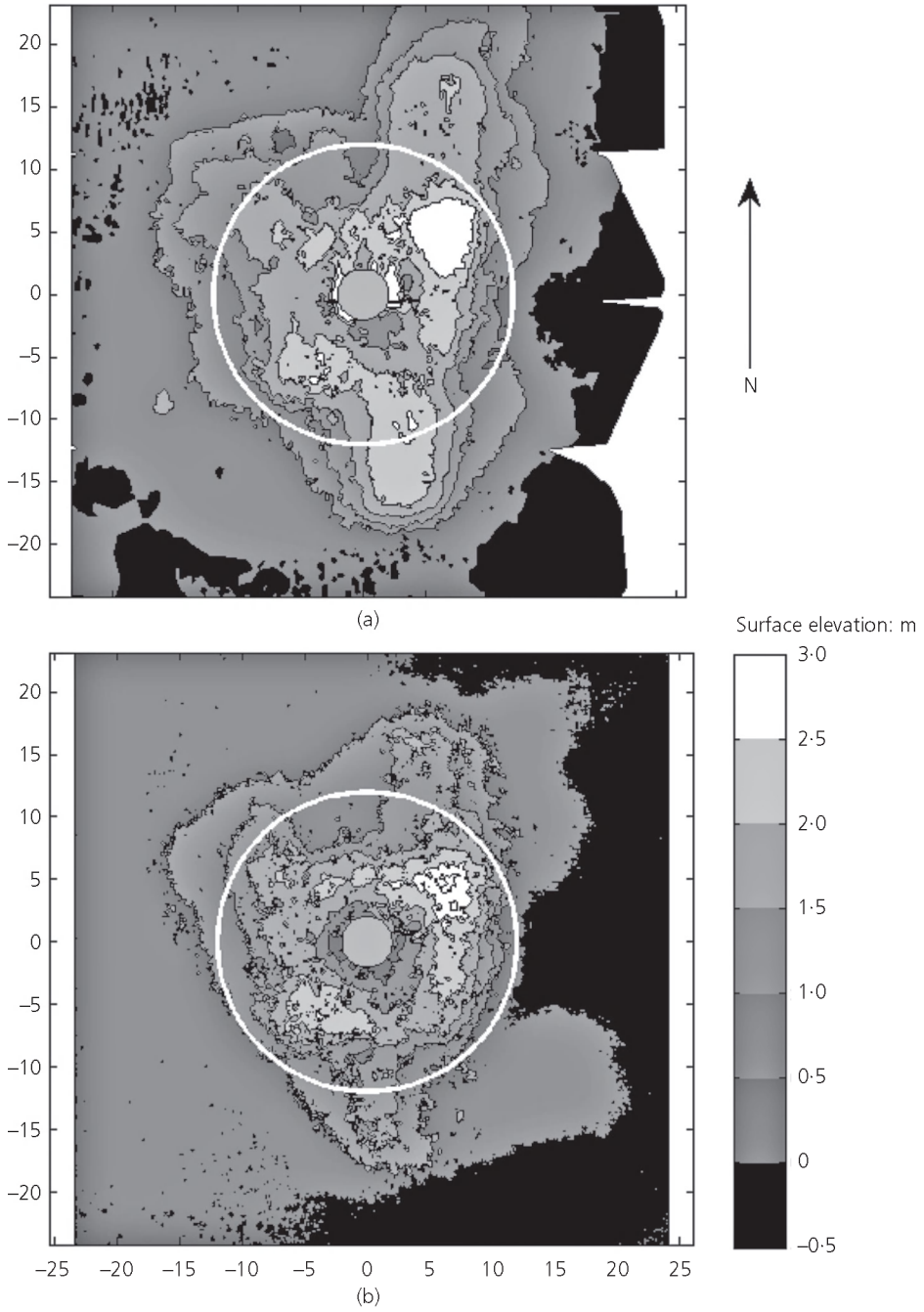

Figure 2. Horns Rev 1 (Denmark). Results of surveys at Turbine 44: (a) 2002 survey; (b) 2005 survey. White circle: design limit of scour protection. Scale to right: surface elevation (bed or scour protection) in metres (Nielsen, 2011)

protection layer, while Figure 4(b) illustrates a multi-layer scour protection where the top horseshoe vortex with a limited penetration depth drives the bottom vortex underneath.

Figures 5 and 6 display the measured mean velocity and turbulence profiles inside the scour protection, respectively, obtained in Nielsen (2011), with and without a filter layer (circles without the filter layer and crosses with the filter layer). The exact location where the data are taken is given in the figure captions. This location is not at the point where the pile-generated adverse pressure gradient is largest (see point A later in Figure 16), but rather at 9·9 cm upstream of that point,

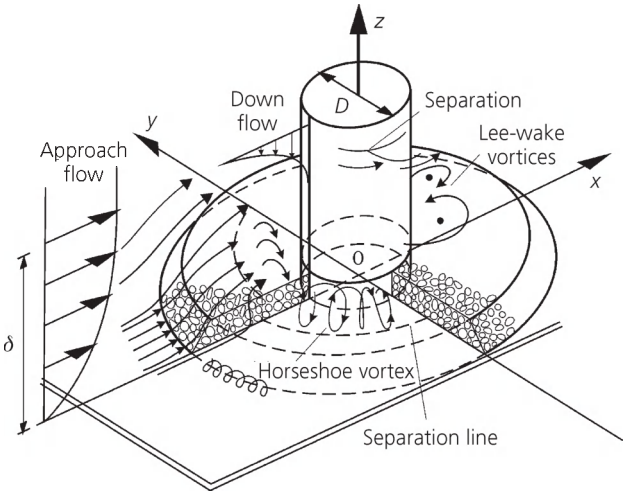

Figure 3. Schematic description (Nielsen *et al.*, 2011)

corresponding to $x = -19$ cm. The pile-generated adverse pressure gradient and its maximum value will be discussed in detail in Section 6.2. The current velocity in these tests was 40 cm/s and the flow depth was 30 cm for one- and two-cover layer cases, and 45 cm for four-cover layer cases (Nielsen, 2011: p. 51). The quantity u is the mean streamwise velocity, and k is the turbulent kinetic energy, defined by

$$k = \tfrac{1}{2}(\overline{u'}^2 + \overline{v'}^2 + \overline{w'}^2) \quad (1)$$

in which $\overline{u'}^2$ is the mean-square value of the fluctuating component of u, and so on. The role of the filter layer is described as follows.

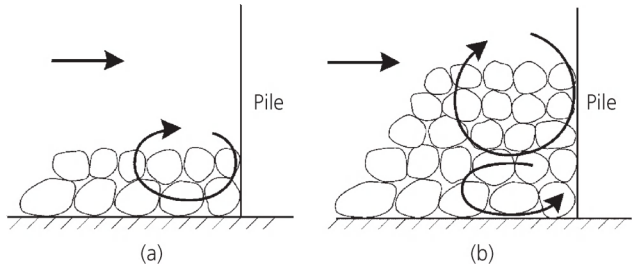

Figure 4. Schematic illustration of flow inside the scour protection (Nielsen *et al.*, 2011)

(*a*) In the case of the one-cover layer, the mean velocity profile in the flow-reversal region is displaced upward with the introduction of the filter, and the near-bed velocity is reduced (Figure 5). (The reverse flow here is essentially the upstream-directed flow of the horseshoe vortex inside the scour protection; see the illustration in Figure 4(a).)

(*b*) In the case of two- and four-cover layers, the role of the filter layer is not as described above. By contrast, the upstream-directed flow of the horseshoe vortex is rather weak in the case of the two-cover layer without the filter, and it essentially changes direction in the case of the four-cover layer (see the illustration in Figure 4(b) for the latter). The near-bed mean flow actually remains practically unchanged when the filter layer is introduced (Figure 5), simply because the thickness of the cover layer in these two cases is too large.

(*c*) Regarding the turbulent-kinetic-energy profiles, Figure 6 clearly shows that the turbulence is reduced quite considerably near the base bottom (Figure 6) for one- and

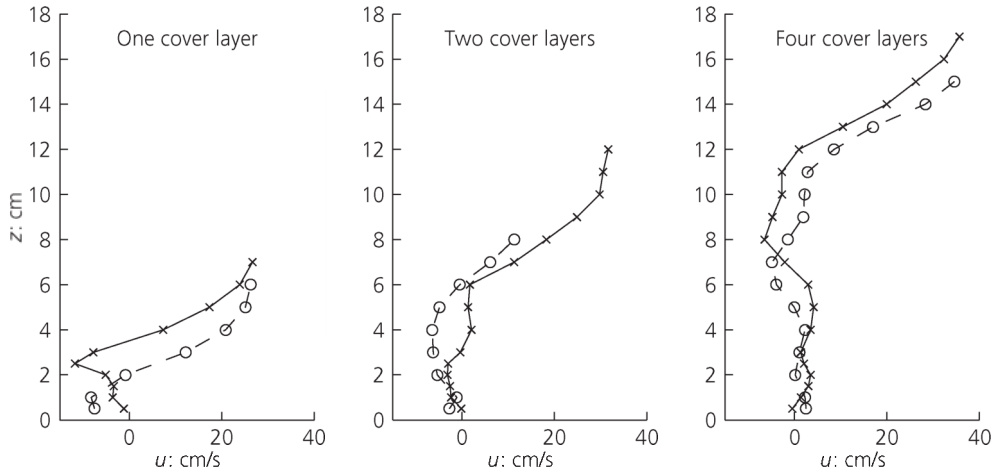

Figure 5. Mean velocity profiles at 12 cm upstream from the leading edge of the $D_p = 14$ cm pile inside the scour protection (i.e. the data are taken at the location $x = -19$ cm, x being measured from the centre of the pile, Figure 3). z is the vertical distance from the rigid base bottom. Circles: without a filter layer. Crosses: with a filter layer. Cover stone size: $D_{c,50} = 4{\cdot}3$ cm. Filter layer of thickness 2 cm with filter stone size $D_{f,50} = 1{\cdot}1$ cm (Nielsen, 2011)

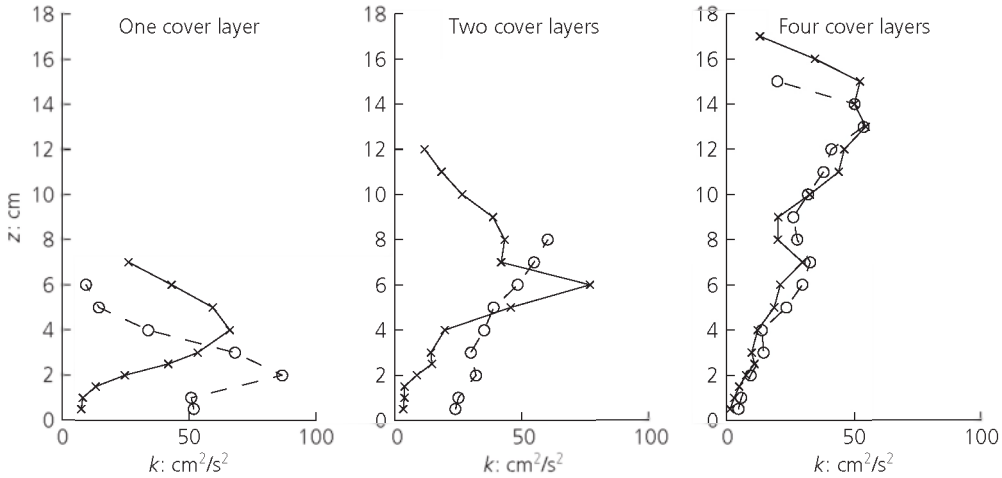

Figure 6. Profiles of turbulent kinetic energy at 12 cm upstream from the leading edge of the $D_p = 14$ cm pile inside the scour protection (i.e. the data are taken at the location $x = -19$ cm, x being measured from the centre of the pile, Figure 3). z is the vertical distance from the rigid base bottom. Circles: without a filter layer. Crosses: with a filter layer. Cover stone size: $D_{c,50} = 4{\cdot}3$ cm. Filter layer of thickness 2 cm with filter stone size $D_{f,50} = 1{\cdot}1$ cm (Nielsen, 2011)

two-cover layers, as expected. The reduction in the turbulence is largest for the one-cover layer case. As for the four-cover layer case, however, the turbulence level is already very small without the filter layer, and it remains unchanged (very small level of turbulence) with the introduction of the filter layer because of the very large thickness of the protection layer.

Although no wave and combined wave and current measurements were made in Nielsen's (2011) study, drawing an analogy to flow around a pile without scour protection (Sumer *et al.*, 1997), it can be inferred that the horseshoe vortex *in the case of waves* is expected to be small. The horseshoe vortex may not even be formed, owing to small values of the Keulegan–Carpenter number in the present case (Sumer *et al.*, 1997), $KC < O(10)$ in which KC is defined by

$$KC = \frac{U_m T}{D_p} \tag{2}$$

where U_m is the maximum value of the far-field orbital velocity of water particles at the bed, T is the wave period and D_p is the pile diameter. This is chiefly because of the very small boundary layer thickness in the case of waves, $O(10\text{ cm})$ at most, in the field. Here, the symbol O means order of magnitude.

In *the case of current and waves*, the picture described for currents is expected to remain essentially practically unchanged even for very small values of the current-to-wave-velocity ratio, U_c/U_m, simply because of the presence of the current boundary layer, and more importantly, because of the presence of a low-momentum region inside the scour protection, which will respond to the adverse pressure gradient generated by the pile, creating a similar horseshoe-vortex flow. In this context, it is interesting to note that, for the 'plain' pile case, Sumer *et al.*'s (1997, see Figures 10, 13 and 16 later) study showed that the horseshoe-vortex flow resembles that in the current-alone case for the values of the current-to-wave-velocity ratio, U_c/U_m, as small as 0·5. It may be expected that, in the present scour-protection case, the horseshoe-vortex flow will remain practically unchanged for even smaller values of U_c/U_m, like $O(0{\cdot}1)$. Although based on physical considerations only, and with no direct evidence, it may be stated that the horseshoe-vortex flow inside the scour protection will resemble that of the current-alone case when $U_c/U_m > O(0{\cdot}1)$.

2.2 Lee-wake vortex flow

Figures 7 and 8 display the results of velocity measurements inside a one-layer scour protection in front of the pile (Figure 7) and behind the pile (Figure 8) obtained in the same test. Note that the velocity scales in the two figures are different.

From the figures, it can be clearly seen that the maximum velocity inside the scour protection in the lee-wake area behind the pile is $O(5\text{ cm/s})$, whereas that in front of the pile, in the horseshoe-vortex area, is of the order of magnitude $O(20\text{ cm/s})$. This is an important point to note.

No wave and combined wave and current measurements were made in Nielsen's (2011) study in the lee-wake area. This is mainly because no significant sinking occurred in the lee-wake area in the sediment-bed tests of Nielsen's (2011) study. This point will be discussed again later.

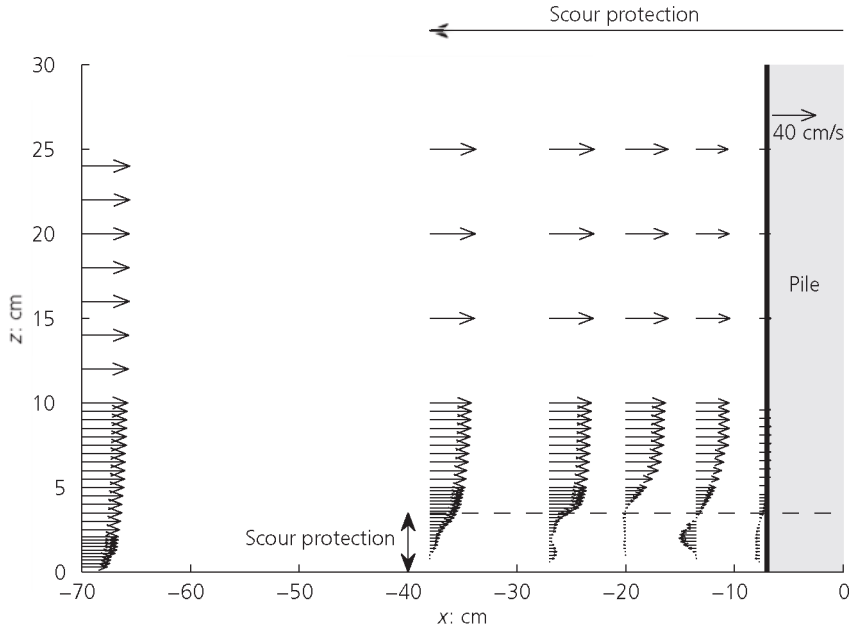

Figure 7. Velocity profiles inside a one-layer scour protection with stones sized 4·3 cm in front of the pile. Note the velocity scale top right (Nielsen *et al.*, 2011)

2.3 Side flow

The flow towards the side of the pile takes place in a convergent geometry. This convergent geometry creates a large, 'favourable' pressure gradient over the pile surface at the sides, with the contraction of streamlines, combined with the presence of the horseshoe-vortex flow, resulting in concentration of flow near the pile. To illustrate the latter, two figures borrowed from Sumer *et al.* (1997) are included in Figures 9 and 10 where the amplification of the bed shear stress around a circular 'plain' pile is given in the form of a contour plot, with a very broad range of the Keulegan–Carpenter number, $KC = 2{\cdot}8$ to $20{\cdot}1$ in Figure 9, and with $KC = \infty$, the current case, in Figure 10.

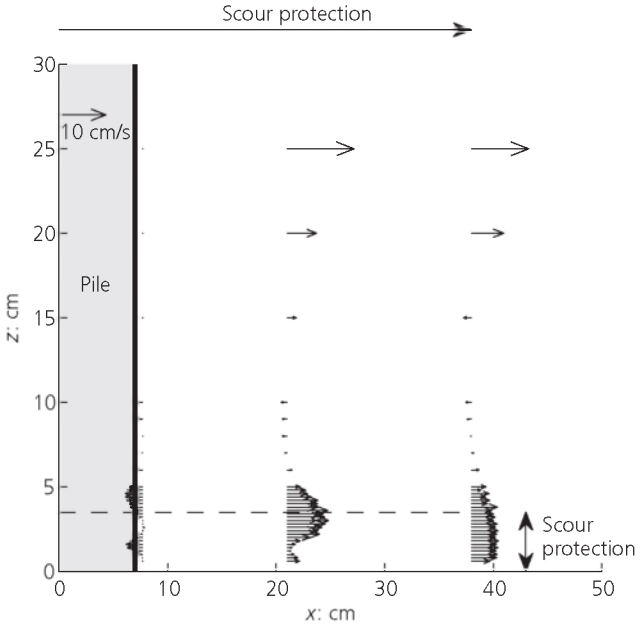

Figure 8. Velocity profiles inside a one-layer scour protection with stones sized 4·3 cm behind the pile. Note the velocity scale top left (Nielsen *et al.*, 2011)

From the figures, the following can be noted. First, although the undisturbed bed shear stress is amplified by as much as a factor of 5 in the horseshoe vortex area in the current case (Figure 10), this amplification is even higher, as much as 11, at around 45° from the stagnation point (Figure 10). This point will be addressed again later. This area is associated with the combined effect of contraction of streamlines and the horseshoe vortex where the swirling horseshoe vortex around the pile eventually trails off downstream. Second, the amplification of the bed shear stress in the lee-wake area in the current case is fairly small (Figure 10), consistent with the result discussed in conjunction with Figures 7 and 8. Third, the amplification of the bed shear stress in the case of waves (Figure 9) is generally substantially smaller than that in the case of current (Figure 10).

3. Initiation of sand motion beneath scour protection

Consider a scour protection consisting of armour stones over a sand bed with filter stones between the armour cover and the

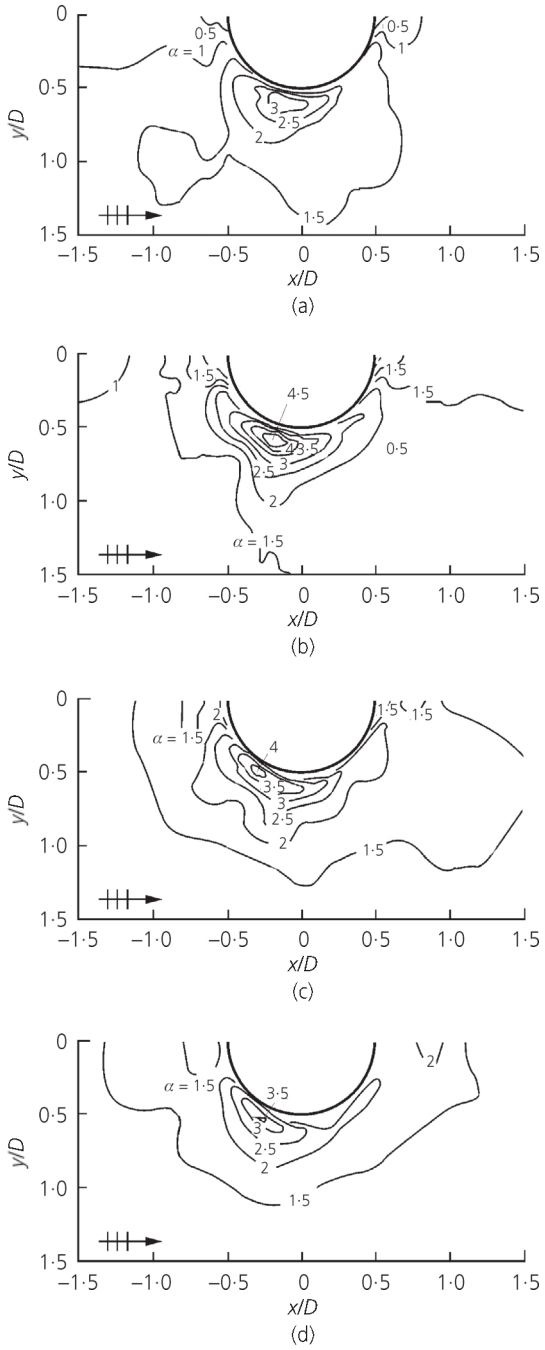

Figure 9. Amplification of the bed shear stress around a circular, 'plain' pile. Waves, $KC = 2{\cdot}8$ to $20{\cdot}1$ (Sumer *et al.*, 1997): (a) $KC = 2{\cdot}8$; (b) $KC = 6{\cdot}1$; (c) $KC = 10{\cdot}3$; (d) $KC = 20{\cdot}1$. Copyright Cambridge University Press

sand bed. Increase the flow velocity. When the velocity reaches a certain point, the sand particles beneath the filter stones begin to move, the so-called initiation of motion, similar to the notion of initiation of motion in sediment transport. From Figure 10, it may be inferred that the initiation of motion first begins at the sides, possibly at around 45°, and in front of the pile.

Nielsen (2011) made an extensive series of experiments where the initiation of motion of small plastic particles (with very small specific gravities) introduced onto the base bottom was observed through the glass bottom of the experimental flume, using a large-scale set-up. This was done at the areas where the bed shear stress is largest in front of the pile. It is important to note that no sediment layer was present in these experiments; the scour protection (with or without the filter layer) was placed on the rigid, glass bottom of the flume. The test conditions in Nielsen's experiments will be given later in the section.

Now, on dimensional grounds, the initiation of motion of the base sand in the field can be described by the following non-dimensional parameters

$$\Omega_{cr} = f\left(\mathrm{Re}_g, N_c, N_f, \frac{D_c}{D_p}, \frac{D_f}{D_p}\right) \tag{3}$$

in which Ω_{cr} is the critical value of the mobility parameter Ω, corresponding to the initiation of motion of the sediment beneath the scour protection in which Ω is defined by

$$\Omega = \frac{U_\infty^2}{g(s-1)D_b}\frac{1}{D_p}D_f\frac{n_f}{1-n_f} \tag{4}$$

In Equation 3, Re_g is the grain Reynolds number corresponding to the bed sediment

$$\mathrm{Re}_g = \frac{U_\infty D_b}{\nu} \tag{5}$$

in which U_∞ is the approach flow velocity, D_b is the bed sediment size and ν is the kinematic viscosity of water. The quantity N_c in Equation 3 is the number of armour stones (cover) layers, defined by

$$N_c = \frac{t_c}{D_c} \tag{6}$$

N_f is the number of filter layers, defined by

$$N_f = \frac{t_f}{D_f} \tag{7}$$

in which t_c and t_f are the thickness of the armour (cover) layer, and that of the filter layer, respectively, D_c is the armour (cover) stone size, D_f is the filter stone size, while D_p is the pile size. In Equation 4, s is the specific gravity of sediment grains, g is the acceleration due to gravity and n_f is the porosity of the filter (appearing in Equation 4 in the form of $n_f/(1-n_f)$; see the next paragraph for the physical meaning of the latter quantity).

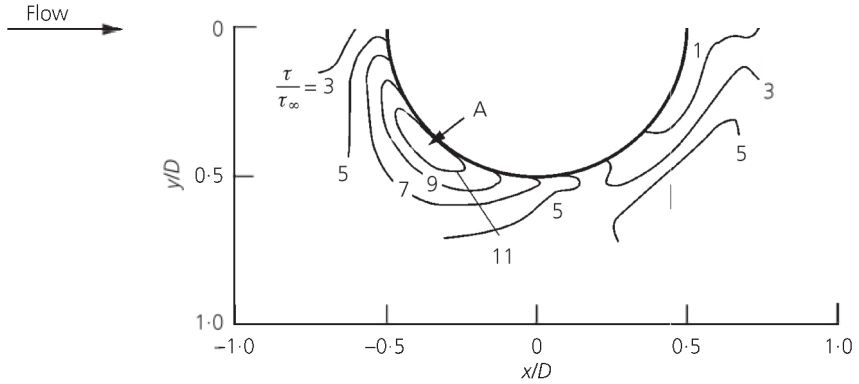

Figure 10. Amplification of the bed shear stress around a circular, 'plain' pile. Current, $KC = \infty$ (Sumer *et al.*, 1997)

It should be noted that the flow through the scour protection (armour and filter layers) occurs in the turbulent regime, and therefore the Reynolds number associated with this flow is not included in the above non-dimensional formulation. The large- and medium-scale experiments conducted in Nielsen's (2011) study satisfy the latter condition, with even the smallest filter stone size being $D_f \gtrsim 1$ cm. With the latter filter stone size, considering the velocity in the pores as being like O (1 cm/s), the grain Reynolds number will be larger than $O(100)$ in Nielsen's experiments. This Re number is large compared with $Re_{cr} = 20$, the critical Re number below which the flow around a sphere occurs in the so-called creeping flow regime. (The authors note that the corresponding field Reynolds numbers are evidently an order of magnitude larger than that experienced in the laboratory.) Considering also that filter stones will, for the most part, have sharp-edged shapes, it may be concluded that the role of the Reynolds number associated with the flow around individual members of stone protection (for both the filter layer and the cover layer) will not be very significant, and therefore can be omitted.

The mobility number in Equation 4, Ω, is an extended version of the familiar Shields parameter; the friction velocity in the Shields parameter is replaced by the approach velocity for convenience. Also, the product $D_f n_f/(1 - n_f)$ represents the 'void ratio' associated with the filter stone size; the larger the value of this quantity, the more susceptible the base sediment to the incipient motion. Likewise, the non-dimensional quantity formed by U_∞, g and D_p in Equation 4, namely $(U_\infty^2/g)/D_p$, represents the adverse pressure gradient in front of the pile, or the pressure gradient over the surface of the pile discussed previously in Section 2 above, the agitating force; the larger the value of this quantity, the larger the mobility of the base sediment.

The grain Reynolds number, Re_g, in Equation 3 is involved because the initiation of motion is also governed by this quantity, reflecting the degree of the embedment of the sand grains in the viscous sublayer, in the same way as in the familiar Shields diagram of the initiation of motion at the bed.

The number of armour layers, N_c, and that of filter layers, N_f, should also be involved because these quantities along with their corresponding stone sizes, D_c/D_p and D_f/D_p, are central in the penetration of the horseshoe-vortex flow and the side flow inside the scour protection. Here the cover/armour stone size and the filter stone size are normalised by the pile diameter.

Figure 11 displays the initiation-of-motion data extracted from Nielsen (2011). The data presented in Figure 11 are selected from Nielsen's (2011) overall data such that the values of the non-dimensional parameters that govern the initiation of motion match with (or close to) those in the field, with $N_c = 2$, $N_f = 9$, $D_c/D_p = 0{\cdot}08$ to $0{\cdot}09$ and $D_f/D_p = 0{\cdot}02$, corresponding to the selected set of data (see legend of Figure 11). (This point will be revisited later in conjunction with the check for sand motion beneath scour protection in the Horns Rev 1 case.) The test conditions (Nielsen, 2011) for the data plotted in Figure 11 are summarised in Table 1. It is noted that experimenting with the pile, the size $D = 1$ m (see the last row in Table 1) will be at the expense of a blockage effect, as the pile diameter in this case is not small. From the potential flow theory, this blockage effect is estimated to be less than 7%, meaning that the velocities in this experiment will be increased slightly, by a small amount, similar to the latter figure. When inspected closely, no clear trend is observed, however, of any blockage effect in Figure 11, and, if anything, it seems that this effect is overshadowed by the scatter in the data.

The large scatter in Figure 11 is due to the random orientation of the pores in the scour protection and the random position of the location on the bottom where the particle was released. (By the random position, it is meant that the particle release position in the pore is random with respect to the pore geometry.) Nevertheless, the data exhibit a fairly well-defined trend.

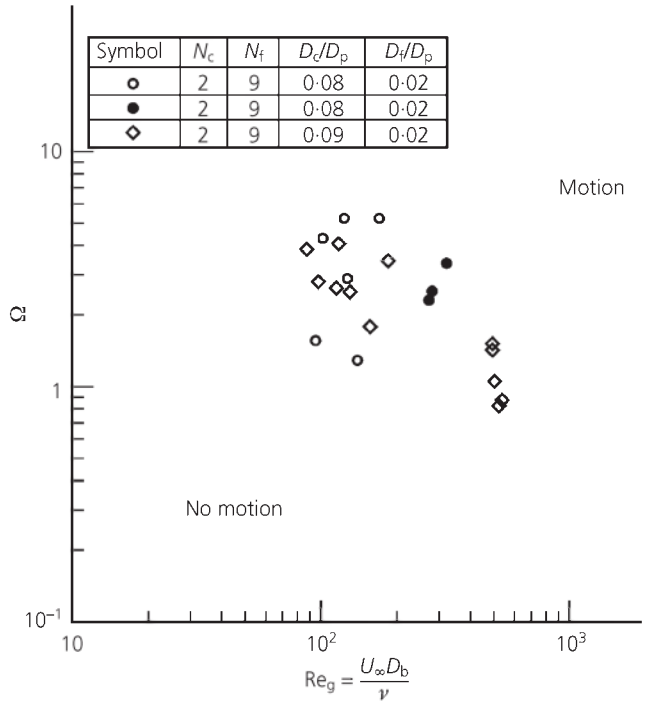

Figure 11. Initiation of motion of sand beneath scour protection around foundation of offshore wind turbine. Current. Data extracted from Nielsen (2011) such that the values of the non-dimensional parameters governing the initiation of motion (see the legend in the figure) match with (or close to) those in a typical application to offshore wind farms

According to this trend, the critical mobility number decreases with increasing $\mathrm{Re_g}$. This is not unexpected. The critical value of the mobility number decreases because the particles beneath the filter layer are more and more exposed as $\mathrm{Re_g}$ increases, and therefore they will be more susceptible to the agitation of the flow.

The area above the trend in Figure 11 corresponds to the 'motion' regime, and that below corresponds to the 'no-motion' regime. The diagram in Figure 11 can be used as a first screening to check whether the sand beneath the scour protection can move or not, as will be demonstrated later for the case of Horns Rev 1.

The range of the parameters used in Figure 11 is given in the figure legend for N_c, N_f, D_c/D_p, and D_f/D_p. The range of $\mathrm{Re_g}$, on the other hand, is $\mathrm{Re_g} = 80$ to 550. Clearly, caution must be observed when using the given diagram outside the indicated range of the parameters. For the test conditions corresponding to the actual tests, the reader is referred to Table 1.

3.1 Discussion of other parameters influencing the initiation of motion

There are other parameters which can influence the initiation of motion. The water depth is one potential parameter when considering very shallow waters. This is because the horseshoe vortex is influenced by this parameter. Unless the water-depth-to-pile-diameter ratio, h/D_p, is smaller than $O(4)$, the effect of this parameter will not, however, be significant (Sumer and Fredsøe, 2002: Figure 3.4). The latter publication shows that the size of the horseshoe vortex decreases with decreasing h/D_p, meaning that the mobility of sand grains decreases with decreasing h/D_p. It may be noted, however, that the reduction in the size of the horseshoe vortex is only 20% even with a water-depth-to-pile-diameter ratio as small as $h/D_p = 1$ (Sumer and Fredsøe, 2002: Figure 3.4). Therefore, although neglecting the influence of the water depth will be slightly on the conservative side, this effect may be ignored for all practical purposes.

Another parameter is the effect of waves. In *the case of waves alone*, the initiation of motion will be much delayed because the agitating flow features such as the horseshoe vortex and the concentration of flow at the sides are significantly smaller than in the case of currents. (Recall the discussion in Section 2 in conjunction with waves; see Figures 9 and 10.) Therefore, the wave-alone case is insignificant, as far as the initiation of motion is concerned. It must be pointed out, however, that the effect of steady streaming, which may be induced by waves similar to Sumer and Fredsøe (2001), is unknown.

Symbols in Figure 11	Pile diam., D_p: m	Cover stone size, D_c: cm	Cover layer thickness, $t_c = N_c D_c$: cm	Filter stone size, D_f: cm	Filter layer thickness, $t_f = N_f D_f$: cm	Approach velocity, U_∞: cm/s	Bed sediment size, D_b: mm	Specific gravity of bed sediment, s
○	0·55	4·3	8·6	1·1	10	16·5–28·4	0·49–0·85	1·045
●	0·55	4·3	8·6	1·1	10	44·2–52·9	0·62	1·310
◇	1·0	9·0	18·0	2·3	20	18·5–25·7	0·44–2·45	1·045

Table 1. Test conditions corresponding to the laboratory data plotted in Figure 11. Water depth was $h = 0{\cdot}9$ m, and the flume width was 3·0 m (Nielsen, 2011)

The effect of *waves, when superimposed on a current*, will be similar to the case of waves alone when the current-to-wave-velocity ratio is very small, like $U_c/U_m < O(0{\cdot}1)$; see the discussion in Section 2.1. Otherwise, the effect of a wave will probably be to increase the agitation owing to the phase-resolved component of the wave. Hence it is expected that the initiation of sand motion at the base bottom will start earlier than in the current-alone case. In the absence of data, therefore, caution should be observed when checking the initiation of the motion based on the current-alone data.

4. Sand motion beneath scour protection and resulting sinking

When the mobility number is larger than the critical value (Figure 11), $\Omega > \Omega_{cr}$, the sand will begin to move. The mechanism of sediment motion involves the flow inside the scour protection discussed in Section 2. The sediment is stirred up by the mean and turbulence components of the flow (Figures 5 and 6), and removed off the bed, and the mean component of the flow inside the scour protection (Figures 4 and 5) will carry the sediment away. The end result is the sinking of the entire scour protection, as discussed in Section 1. In the presence of waves in a combined current and wave environment, the phase-resolved component of the flow inside the scour protection will help further agitate the sand on the bed. The mechanism of sediment motion and the resulting sinking, however, will largely be unaffected.

As in the case of the initiation of motion, the sinking is, for the most part, expected to take place more strongly in front of the pile and at the sides. See the discussion in the preceding section.

Let e_{max} be the maximum equilibrium sinking of the scour protection. On dimensional grounds, this quantity is described by the following non-dimensional parameters

$$\frac{e_{max}}{D_c} = f\left(\Omega, \mathrm{Re}_g, N_c, N_f, \frac{D_c}{D_p}, \frac{D_f}{D_p}\right) \tag{8}$$

in which e_{max} is normalised by the armour stone size, D_c.

Nielsen (2011) carried out extensive experiments with a sand bed with scour protection, where he measured the sinking of the scour protection. He did two kinds of experiments, as follows.

(*a*) Experiments were conducted without filter stones where the current was strong enough to cause sediment motion underneath the scour protection and therefore sinking of the protection layer.
(*b*) He repeated these experiments in a limited number of tests where filter stones also were used. Of the six tests conducted with filter stones, three tests had a cover stone size of $D_c/D_p = 0{\cdot}4$ to $0{\cdot}5$, too large a value to represent a typical field situation. Therefore, these three tests will not be considered in the present analysis.

Incidentally, Nielsen (2011: p. 14) reports that, in his sediment bed experiments, the sinking took place in front of and along the sides of the pile adjacent to the scour protection. This is obviously not unexpected, and it is consistent with the discussion in the preceding paragraphs.

Figure 12 presents data from Nielsen's (2011) experiments, plotted according to the non-dimensional formulation given in Equation 8. The set of data plotted in Figure 12 is selected so

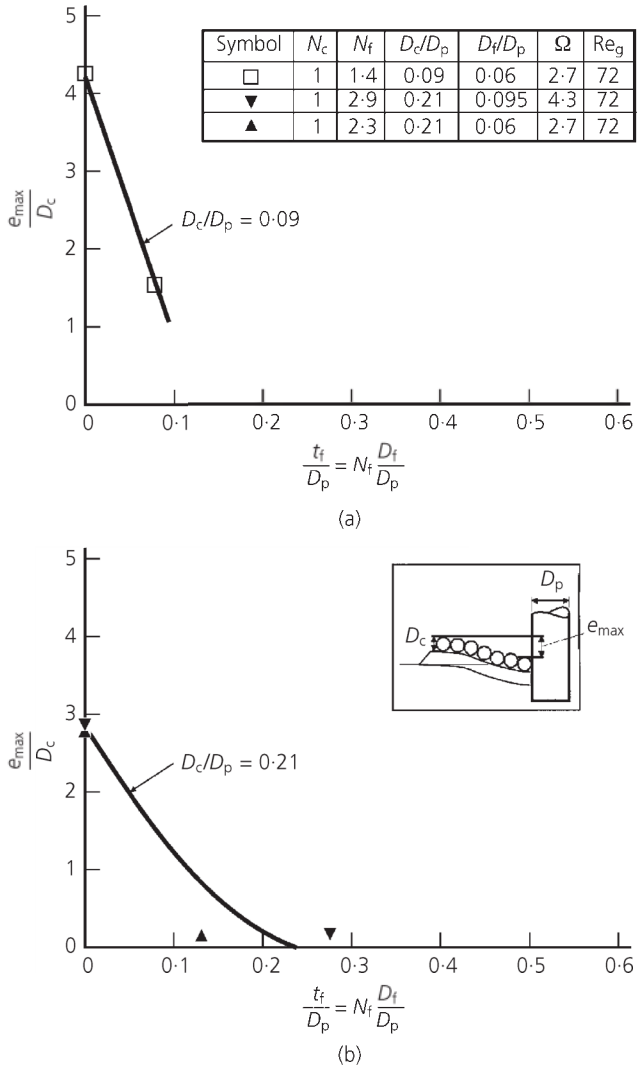

Figure 12. Maximum sinking of scour protection. The origin of the horizontal axis, $t_f/D_p = 0$, corresponds to the no-filter case. The filter-case symbols (see the legends) are also used for the no-filter case as well, for convenience. Data extracted from Nielsen's (2011) data; data for $t_f/D_p = 0$ are taken according to the best-fit line through the data

that the test conditions are closest to typical conditions encountered in OWFs; the order of magnitude values of typical conditions in the field may be summarised as $N_c = O(2)$, $N_f = O(10)$, $D_c/D_p = O(0{\cdot}1)$, and $D_f/D_p = O(0{\cdot}01)$. The test conditions corresponding to the data plotted in Figure 12 are given in Table 2. It is noted that Nielsen (2011) (also reported in Nielsen *et al.*, 2011: Figure 11) gives the entire set of data for the no-filter experiments, plotted in the form of e_{max}/D_c against D_p/D_c, with N_c taking the values of 1, 2 and 3.

Figure 12 illustrates very clearly the role of the filter used in scour protection. The figure shows that the sinking of scour protection with an armour cover with $D_c/D_p = 0{\cdot}09$ is drastically reduced from $e_{max}/D_c = 4{\cdot}5$ to $1{\cdot}5$ by introducing filter stones with $t_f/D_p \cong 0{\cdot}1$. Likewise, the sinking in the case of $D_c/D_p = 0{\cdot}21$ is even more dramatically reduced from $e_{max}/D \cong 3$ to about $0{\cdot}2$ by introducing filter stones with $t_f/D_p \cong 0{\cdot}2$. Clearly, the latter results are linked to the reduction of the agitating forces with the introduction of the filter stones, as discussed in Section 2 (see Figures 5 and 6).

Nielsen (2011) carried out a small number of experiments with waves. Two of the wave tests (Nielsen, 2011: tests 6 and 10, Table 7.1) are selected such that the properties of the scour protection match with those corresponding to the current case presented in the previous figure so that comparison can be made on the same basis. The data are plotted in Figure 13 where the properties of scour protection as well as the sediment are the same as in the current tests, with the exception that no filter existed in the wave case. The Keulegan–Carpenter number was $KC = 1{\cdot}5$ in one test, and 4 in the other (the upper and lower data points, respectively, in Figure 13). Nielsen (2011: p. 122) reports that the maximum sinking occurred near the sides, adjacent to the pile, as opposed to the current case where the maximum sinking occurred both in front of and along the sides of the pile.

Even with the absence of the filter stones in the wave tests, the sinking is apparently small compared with that in the current

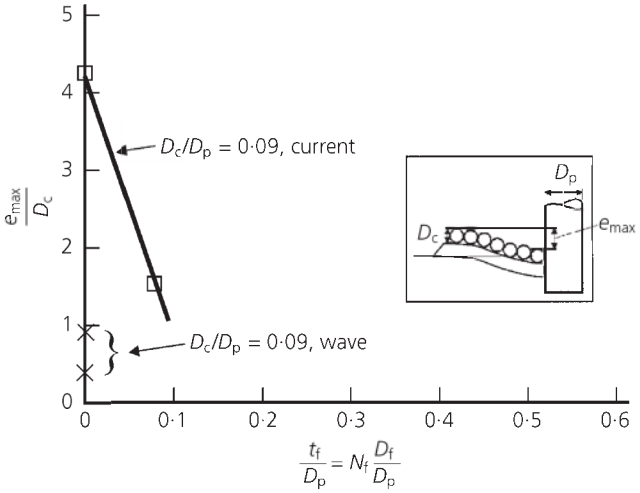

Figure 13. Wave-induced sinking compared with current-induced sinking

(Figure 13), the general trend observed in the limited number of tests in Nielsen's (2011) study. This is linked to the fact that the horseshoe vortex is very weak owing to the small boundary layer thickness in waves, and furthermore the amplification of the bed shear stress in the case of waves (Figure 9) is substantially smaller than that in the case of current (Figure 10). It is to be noted, however, that the sinking pattern may change substantially in the case of combined waves and current, with larger sinking resembling more closely that experienced in the current-alone case. Also, the location of sinking of the stones may differ from current-alone and wave-alone cases, depending on the wave-current climate. However, no data are yet available to substantiate this.

5. Horns Rev 1 case. Sand motion beneath scour protection and resulting sinking

The purpose of this section is to test and validate the previously mentioned new findings from Nielsen's study (2011) against the Horns Rev 1 case, to gain confidence in the use of this information in practice.

Symbols in Figure 12	Pile diam. D_p: m	Cover stone size D_c: cm	Cover layer thickness $t_c = N_c D_c$: cm	Filter stone size D_f: cm	Filter layer thickness $t_f = N_f D_f$: cm	Approach velocity U_∞: cm/s	Bed sediment size D_b: mm
□	0·20	1·9	1·9	1·1	1·5	0·40	0·18
▼	0·20	4·3	4·3	1·9	5·5	0·40	0·18
▲	0·20	4·3	4·3	1·1	2·5	0·40	0·18

Table 2. Test conditions corresponding to the laboratory data plotted in Figure 12. Water depth was $h = 0{\cdot}56$ m and the flume width 4·0 m (Nielsen, 2011)

Pile diameter, D_p: m	Cover stone size, D_c: m	Cover layer thickness, t_c: m	Filter stone size, D_f: m	Filter layer thickness, t_f: m	Bed sediment size, D_b: mm
4·2	0·40	1·0	0·10	0·50	0·5

Table 3. Input parameters, Horns Rev 1 case. Note that all D values in the table are D_{50}

5.1 Initiation of motion beneath scour protection

Table 3 presents the input parameters for the Horns Rev 1 case (Hansen *et al.*, 2007). Three velocity values are adopted in the calculations, $U_\infty = 0{\cdot}88$, 1·0 and 1·5 m/s in which 0·88 m/s is the 50-year-return-period velocity, as mentioned previously (Hansen *et al.*, 2007). The latter authors, however, also state that maximum currents up to 1 m/s may be encountered. The stone sizes and the grain size of the seabed sediment in Table 3 all correspond to D_{50}, the size at which 50% of the sediment weight is finer. The mobility number, Ω, the Reynolds number, Re_g, and other non-dimensional parameters, N_c, N_f, D_c/D_p, D_f/D_p, that govern the initiation of motion beneath scour protection, are calculated, based on the input parameters in Table 3. The calculated values of these parameters for the three different velocities are given in Table 4.

Comparison of the values of the governing parameters in Table 4 with those given in Figure 11 shows that the values practically match, with the exception that the number of filter layers in Horns Rev 1 is $N_f = 5$ whereas that for the data in Figure 11 is $N_f = 9$. Nevertheless comparison can be made, bearing in mind that the N_f in Horns Rev 1 is a factor of 2 smaller than the critical mobility data of Figure 11.

Figure 14 displays the results. In Figure 14, the symbol H represents the mobility for the Horns Rev 1 for the three velocities, $U_\infty = 0{\cdot}88$, 1·0 and 1·5 m/s in Table 4, while the rest of the data in Figure 14 are reproduced from Figure 11.

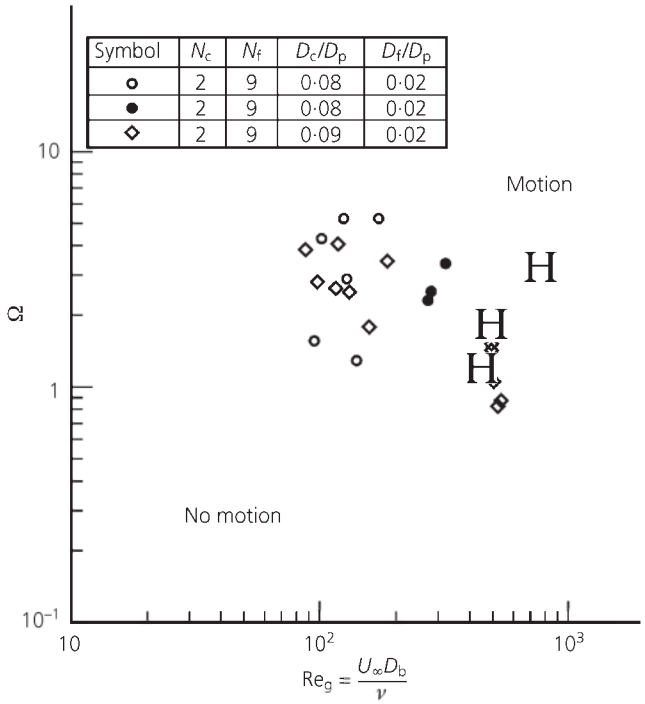

Figure 14. Check for initiation-of-motion on the sediment beneath scour protection, Horns Rev 1 case. Symbol H corresponds to the points for Horns Rev 1, for velocities $U_\infty = 0.88$ m/s (lowermost point), $U_\infty = 1$ m/s (middle point) and for $U_\infty = 1{\cdot}5$ m/s (uppermost point). The values of Ω indicated in the diagram for these three points are: $\Omega = 1{\cdot}2$ with $\mathrm{Re}_g = 440$ for $U_\infty = 0{\cdot}88$ m/s; $\Omega = 1{\cdot}6$ with $\mathrm{Re}_g = 500$ for $U_\infty = 1{\cdot}0$ m/s; and $\Omega = 3{\cdot}6$ with $\mathrm{Re}_g = 750$ for $U_\infty = 1{\cdot}5$ m/s. Rest of data are reproduced from Figure 11, the data corresponding to the initiation of motion of Nielsen (2011)

Figure 14 clearly shows that the sediment underneath the scour protection in Horns Rev 1 is certainly not in the 'no-motion' state, even with the critical mobility data of Figure 11, which are obtained for a filter layer with $N_f = 9$, a value that is a factor of 2 larger than the field value at Horns Rev 1. The analysis in Section 6 in connection with filter criteria will also confirm this finding.

Approach velocity U_∞: m/s	Mobility parameter Ω	Grain Reynolds number, Re_g	Number of cover (armour) layers, N_c	Number of filter layers, N_f	Normalised cover (armour) stone size, D_c/D_p	Normalised filter stone size, D_f/D_p	Thickness of filter layer, t_f/D_p
0·88	1·2	440	2·5	5	0·095	0·02	0·1
1·00	1·6	500	2·5	5	0·095	0·02	0·1
1·50	3·6	750	2·5	5	0·095	0·02	0·1

Table 4. Non-dimensional parameters governing the initiation of motion beneath scour protection, Horns Rev 1 case

	Mobility parameter Ω	Grain Reynolds number, Re_g	Number of cover (armour) layers, N_c	Number of filter layers, N_f	Normalised cover (armour) stone size, D_c/D_p	Normalised filter stone size, D_f/D_p	Thickness of filter layer, t_f/D_p
Symbols in Figure 12(a)	2·7	72	1	1·4	0·09	0·06	0·075
Horns Rev 1	1·6	500	2·5	5	0·095	0·02	0·1

Table 5. Governing parameters for laboratory tests and Horns Rev 1 case

5.2 Sinking of scour protection

As mentioned in the preceding paragraphs, the sinking data with filter stones present, plotted in Figure 12, are very limited, with only three data points. Of these, the top panel is closest to the Horns Rev 1 case, with the cover armour stone size $D_c/D_p = 0{\cdot}09$, which is very much the same as in Horns Rev 1 (Table 4). Yet, it is noted that there are significant differences between the values of the governing parameters in Nielsen's (2011) experiments (Figure 12(a), Table 5) and in Horns Rev 1 case (Tables 4 and 5). Therefore comparison between the reported sinking at Horns Rev 1 and Figure 12(a) should be treated with extra caution. Nevertheless, comparison is presented in Figure 15 where the standard deviation sign represents the range of the observed sinking at Horns Rev 1, namely from practically zero up to 1·5 m, or alternatively, when scaled with the armour cover stone size, $e_{max}/D_c = 0$ to 3·8. Although there are significant differences between the values of the governing parameters, the two sets of data appear to lie over the same range.

6. Filter criteria

6.1 A design approach

A detailed design strategy for the filter layer may be adopted, following the work of de Graauw *et al.* (1984). This is summarised below.

First, determine $D_{f,85}$ of the filter material from

$$D_{c,15} < 5D_{f,85} \tag{9}$$

(known as the Terzaghi criterion) in which $D_{c,15}$ corresponds to 15% of the armour/cover weight being finer. This criterion is essentially based on geometrical considerations. The armour stone size is, by definition, large compared with the filter stone size, but nevertheless, it should not be too large to allow the filter stones to be washed out through the pores of the armour material. The above criterion ensures that the filter stones will not be washed out.

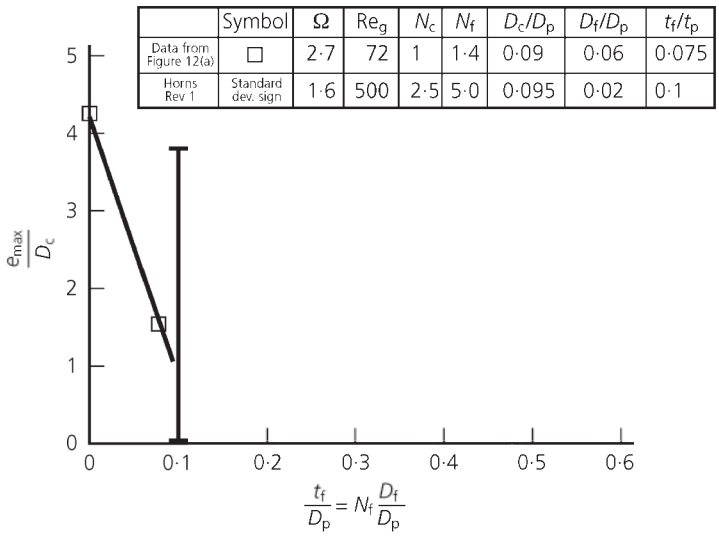

Figure 15. Maximum sinking of scour protection. Comparison between observed Horns Rev 1 and Nielsen's (2011) laboratory data (reproduced from Figure 12(a)). For the laboratory data, the filter-case symbol also is used for the no-filter case ($t_p/D_p = 0$), on the vertical axis

Second, determine $D_{f,15}$ of the filter material from

10. $$I < I_{cr}$$

in which I is maximum hydraulic gradient in the horizontal direction present in the filter layer, and I_{cr} is the critical value of the hydraulic gradient corresponding to the initiation of motion at the interface between the filter layer and the base sand bed. This criterion ensures that the base sand of the size $D_{f,15}$ (and coarser) will not be washed out as a result of the flow that takes place inside the filter layer (see Section 2). The quantity I_{cr} is given by de Graauw *et al.* (1984) as follows

11. $$I_{cr} = \left(\frac{0.06}{n_f^3 D_{f,15}^{4/3}} + \frac{n_f^{5/3} D_{f,15}^{1/3}}{1000 D_{b,85}^{5/3}} \right) V_{*cr}^2$$

in which n_f is the porosity of the filter material, taken in the present application as 0·35, and $D_{f,15}$ and $D_{b,85}$ are given in metres.

The bed-sediment size in the above equation is taken as $D_{b,85}$ rather than $D_{b,50}$. This is on the recommendation of de Graauw *et al.* (1984), who argue that, in the case of graded base material, it may be assumed that the base material will be better characterised by $D_{b,85}$ (de Graauw *et al.*, 1984: p. 84). Furthermore, the quantity V_{*cr} is the critical shear velocity approximated from the Shields diagram by

12. $$V_{*cr} = 1{\cdot}3 D_{b,50}^{0.57} + 8{\cdot}3 \times 10^{-8} D_{b,50}^{-1.2}$$

for sand in which V_{*cr} is in metres per second and $D_{b,50}$ is in metres. Equation 12 given by de Graauw *et al.* (1984) actually represents the critical curve (corresponding to the initiation of motion) in the familiar Shields diagram where the grain size is the mean sediment size (Shields, 1936).

The above criterion, Equation 11 given in de Graauw *et al.* (1984), was based on their extensive experiments *under steady current conditions*.

6.2 Horizontal hydraulic gradients in currents

There are two kinds of horizontal hydraulic gradients which are potentially capable of moving the base sediment at the bed underneath the filter layer

(*a*) hydraulic gradient in front of the pile
(*b*) hydraulic gradient over the surface of the pile.

These hydraulic gradients are, from the potential flow theory (Sumer *et al.*, 1997), given as follows (see Figure 16 for definition sketch).

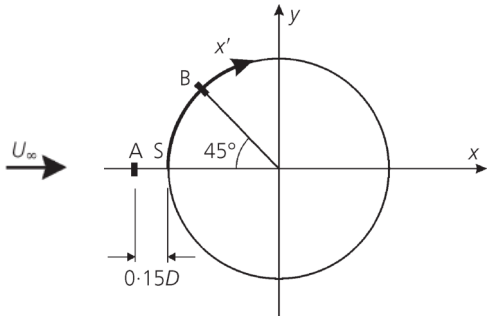

Figure 16. Definition sketch. Point S: stagnation point. Point A: location where the horizontal hydraulic gradient in front of the pile (the adverse pressure gradient) becomes maximum. Point B: location where the horizontal hydraulic gradient over the surface of the pile (the favourable pressure gradient) becomes maximum

First, the horizontal hydraulic gradient in front of the pile (the upstream-directed, adverse pressure gradient that drives the horseshoe vortex system)

13. $$I = \frac{\partial(p/\gamma)}{\partial x} = \frac{U_\infty^2}{2g} \frac{1}{D} \left[1 - \frac{1}{4(x/D)^2} \right] \left[\frac{1}{(|x|/D)^3} \right]$$

It can readily be shown that the maximum value of this gradient occurs at a distance 0·15D from the upstream edge of the pile, point A in Figure 16.

Second, the horizontal hydraulic gradient over the surface of the pile (the downstream-directed, favourable pressure gradient over the surface of the pile caused by the 'convergent' geometry of the flow from the stagnation point towards the sides of the pile)

14. $$I = \frac{\partial(p/\gamma)}{\partial x'} = 16 \frac{U_\infty^2}{2g} \frac{1}{D} \sin(2x'/D) \cos(2x'/D)$$

in which x' is the distance over the surface of the pile, measured from the stagnation point (point S in Figure 16). The maximum value of this hydraulic gradient occurs at 45° from the stagnation point, point B in Figure 16.

The above hydraulic gradients can be considered to 'penetrate' through the granular protection layer, and therefore are present at the seabed level. No data are available yet to confirm this assumption. However, there is experimental and theoretical, 'indirect' evidence supporting this assumption (Sumer and Fredsøe, 2002: pp. 484–485; Sumer *et al.*, 2010: p. 870) in the case of waves.

An important point in connection with the above hydraulic gradients is that the hydraulic gradient over the surface of the pile, Equation 14, is a factor of 5 larger than that in front of

the pile, Equation 13 (Sumer *et al.*, 1997). The hydraulic gradient over the surface of the pile is, in real life, associated with the combined effect of contraction of streamlines and the horseshoe vortex where the swirling horseshoe vortex around the pile eventually trails off downstream, as discussed in Section 2 in conjunction with Figure 10.

6.3 Horizontal hydraulic gradients in waves

The horizontal hydraulic gradients, both in front of the pile and over the surface of the pile, in the case of waves can be calculated from MacCamy and Fuchs (1954) potential flow solution, see for example, Sumer and Fredsøe (1997: p. 276). The analytical expressions are somewhat cumbersome, and therefore will not be given here. Only the results (obtained for the horizontal hydraulic gradients at the bed) will be presented in Section 7 where the implementation of the filter criteria is discussed for the Horns Rev 1 case.

7. Filter criteria applied to Horns Rev 1 case

The stone sizes of the scour protection and the sand sizes of the sediment bed for Horns Rev 1 case are reproduced from Hansen *et al.* (2007) in Table 6, including D_{50} values given already in Table 3.

7.1 Terzaghi criterion

For the filter material to remain stable, Equation 9, the Terzaghi criterion, should be satisfied. From Table 6, $D_{c,15} = 370$ mm, and $D_{f,85} = 200$ mm. It can be seen that the Terzaghi criterion, $D_{c,15} < 5D_{f,85}$, is satisfied. Hence the observed failure of the scour protection cannot be linked to the Terzaghi criterion. (For an extensive account of filter criteria (the stability, internal stability and permeability) and the use of filters in hydraulic engineering, the reader is referred to CIRIA/CUR/Cetmef (2007).)

7.2 de Graauw *et al.* criterion

Table 7 lists the horizontal hydraulic gradients obtained from Equations 13 and 14, for three current velocities, $U_\infty = 0{\cdot}88$, 1·0 and 1·5 m/s. On the other hand, taking the stone/grain sizes from Table 6, and the porosity of the filter as $n_f = 0{\cdot}35$, the critical Shields velocity and the critical hydraulic gradient are obtained from Equations 11 and 12, respectively, and the results are given in Table 8.

	D_{15}: mm	D_{50}: mm	D_{85}: mm
Armour cover	370	400	550
Filter	20	100	200
Seabed	0·1	0·5	1·0

Table 6. Scour protection and base sediment, Horns Rev 1 (taken from Hansen *et al.* (2007))

U_∞: m/s	Maximum value of I in front of the pile, from Equation 13	Maximum value of I over the surface of the pile, from Equation 14
0·88	0·014	0·075
1·0	0·018	0·097
1·5	0·040	0·218

Table 7. Maximum values of the horizontal hydraulic gradient: current, Horns Rev 1 case

Comparison between the critical hydraulic gradient (Table 8) and the values given in Table 7 indicates that, with the 1 m/s velocity, the sediment beneath the filter layer will move at areas 45° from the stagnation point (at areas around point B in Figure 16), and therefore the scour protection will fail, a result consistent with Section 5 and Figure 14. (As noted earlier, current velocities up to 1 m/s can occur at Horns Rev 1 (Hansen *et al.*, 2007).)

Direct comparison of the present criterion given in Figure 11 and that of de Graauw *et al.* (1984) is not possible. However, an indirect comparison can be made with reference to the Horns Rev 1 case. The results of the latter are summarised in Table 9. Although the present criterion indicates that the sediment motion is at the threshold for the velocity $U_\infty = 0{\cdot}88$ m/s while de Graauw *et al.*'s criterion indicates that there is no sediment motion for this velocity, both criteria show, however, that there is sediment motion for the other two velocities. No clear explanation has been found for the discrepancy for the velocity $U_\infty = 0{\cdot}88$ m/s. While the present criterion was obtained from a laboratory experiment simulating precisely the same process as in the field (i.e. the initiation of motion beneath the scour-protection filter layer around the foundation of an offshore wind turbine), de Graauw *et al.*'s (1984) criterion was obtained from an experiment where the sediment motion beneath a filter layer was studied in a horizontal pressure gradient field. Despite the completely different experimental settings, it is remarkable that the two criteria give similar results. The current authors believe that the new set of information described in the present paper (including the hydrodynamics described in Sections 2–4) and the filter criteria of de Graauw *et al.* (1984) form a complementary source of information on scour protection with special reference to OWT foundations.

$D_{f,15}$	$D_{b,50}$	$D_{b,85}$	V_*	I_{cr}
20 mm	0·5 mm	1·0 mm	1·8 cm/s	0·083

Table 8. Critical hydraulic gradient; Horns Rev 1 from Equation 11

U_∞: m/s	Present criterion according to Figure 11			de Graauw *et al.*'s (1984) criterion		
	Mobility, Ω	Critical mobility from Figure 11, Ω_{cr}	Is sand underneath the filter in motion? (i.e. $\Omega > \Omega_{cr}$)	Maximum value of hydraulic gradient over the surface of the pile, from Equation 14, I	Critical hydraulic gradient from Equation 11, I_{cr}	Is sand underneath the filter in motion? (i.e. $I > I_{cr}$)
0·88	1·2	~1·2	Critical	0·075	0·083	No
1·0	1·6	~1·2	Yes	0·097	0·083	Yes
1·5	3·6	~0·7	Yes	0·218	0·083	Yes

Table 9. Comparison of the present criterion in Figure 11 and that of de Graauw *et al.* (1984), with reference to the Horns Rev 1 case

Clearly, when applying de Graauw *et al.*'s (1984) criteria, caution must be observed with regard to the hydraulic gradient involved in the formulation of de Graauw *et al.* This has been determined in the present study from a potential-flow approach, Equation 14, and the agreement between the present study and the de Graauw *et al.*'s work implies that this approach is evidently reasonable. However, another approach may be to use directly computed values of the hydraulic gradient from a computational fluid dynamics (CFD) exercise whereby the flow within and around the scour protection layer (and therefore the hydraulic gradient) is calculated.

7.2.1 Discussion of the effect of waves

As pointed out earlier, the two horizontal hydraulic gradients in the case of waves can be calculated, using MacCamy and Fuchs' (1954) solution (e.g. see Sumer and Fredsøe, 1997: p. 276). The maximum values of these hydraulic gradients, obtained from MacCamy and Fuchs' solution, are indicated in Table 10 for the following wave conditions: wave height, the significant wave height, $H = 3{\cdot}5$ m; the wave period, the peak wave period, $T = 10$ s; and the water depth, $h = 10$ m, representing a typical storm condition, as mentioned previously (Hansen *et al.*, 2007: section 4.1.4). For this wave period and water depth, the wave length from the small-amplitude wave theory is found to be $L = 92{\cdot}4$ m.

Maximum value of I in front of the pile at the seabed, from MacCamy and Fuchs (1954) solution	Maximum value of I over surface of pile, at the seabed, from MacCamy and Fuchs (1954) solution
~0·1	0·195

Table 10. Maximum values of the horizontal hydraulic gradient: waves

The MacCamy and Fuchs' solution indicates that the maximum value of the hydraulic gradient over the surface of the pile at the bed occurs at approximately 88° (almost at the sides) from the offshore edge of the pile. This result is consistent with the fact that Nielsen (2011) consistently observed that the sinking of scour protection (albeit small) always occurred at the sides of the pile in the case of waves, contrary to what occurred in currents, namely that the sinking occurred at the sides and in front of the pile.

Comparison between the critical hydraulic gradient (Table 8) and the values given in Table 10 indicates that the sediment beneath the filter layer will move, as $I = 0{\cdot}195$ is considerably larger than the critical value $I_{cr} = 0{\cdot}083$, and this will occur at areas almost at the sides of the pile, as pointed out earlier. Therefore the scour protection will fail at these areas, a result consistent with Nielsen's (2011) experiments in waves. However, see the following discussion.

7.2.2 Discussion of the applicability of Equation 11 in waves

The present authors believe that the applicability of Equation 11 for the waves-alone case may lead to somewhat conservative results for the following reasons. First of all, the de Graauw *et al.* equation, Equation 11, was obtained for steady current conditions, not for waves, and therefore is, in principle, not applicable for waves.

Second, in de Graauw *et al.*'s (1984) study, critical horizontal hydraulic gradients also are determined from oscillatory flow experiments. de Graauw *et al.* (1984) stated that the behaviour of the critical hydraulic gradient was similar to that of currents only during the first cycle of motion. With the completion of the first cycle, the filter resistance was increased, becoming so large that the critical hydraulic gradient became almost unity, $I_{cr} \approx 1$. This is clearly because, with the reversal of the flow, the grains will rearrange, and therefore the filter material will

be compacted, and hence the critical hydraulic gradient will be increased.

Third, the preceding consideration implies therefore that the critical hydraulic gradient for waves alone cannot be approximated by that obtained under current conditions.

It may be argued that the current critical hydraulic gradient, Equation 11, may be used for the first cycle of motion. But obviously, the sinking is a long-term process; even if sediment motion is obtained under the given set of wave conditions, this does not have any significance because the sediment motion will stop in the next cycle because the filter resistance will be increased quite considerably after the first cycle, and therefore no further motion of the sediment will take place, and therefore no sinking of the scour protection.

Fourth, although limited, Nielsen's (2011) experiments indicated that the wave-induced sinking was small compared with that in currents (Figure 13). Therefore, a wave-induced hydraulic gradient like $I = 0{\cdot}195$ (Table 10), causing sediment motion and resulting sinking as opposed to the current-induced hydraulic gradient $I = 0{\cdot}097$ (Table 7), is not consistent with Nielsen's (2011) observations.

Regarding the case of combined waves and current, no study is yet available investigating the initiation of motion and the resulting sinking in combined waves and current, as discussed earlier. As already pointed out, the effect of *wave, when superimposed on a current*, will be similar to the case of waves alone when the current-to-wave-velocity ratio is very small (wave-dominated case); see the discussion in Section 2.1. Therefore, the discussion in the preceding paragraphs for the case of waves alone will be valid for this case, too. When the latter ratio is large, however, larger than $O(0{\cdot}1)$, the horseshoe-vortex flow inside the scour protection will resemble the current-alone case (as discussed in Section 2.1), and therefore the maximum horizontal hydraulic gradient can be calculated from Equation 14, with possibly the approach velocity taken as the sum of the current approach velocity and the wave-induced velocity at the bed, $U_\infty + U_m$. As already stated, no data are available yet to substantiate these physical considerations, and therefore extreme caution must be observed when implementing this recommendation.

7.2.3 What is the filter stone size to satisfy the de Graauw criterion?

With a back calculation, it is possible to work out the filter stone size, $D_{f,15}$, which satisfies the de Graauw criterion. For this, the maximum value of the hydraulic gradient over the surface of the pile from Equation 14 is put equal to the critical hydraulic gradient, Equation 11, and the equation is solved for the filter stone size $D_{f,15}$. This gives a $D_{f,15}$ of 17·8 mm for the velocity $U_\infty = 1{\cdot}0$ m/s. Thus, a filter stone size $D_{f,15}$ equal to or smaller than 17·8 mm will be stable.

8. Discussion

The total sinking at Horns Rev 1 is about 1·5 m. Stability calculations can readily indicate that the armour stones cannot be moved even with the harshest wave and current conditions present at this location. Diver inspection also confirmed that no armour stones were displaced as a result of instability of the armour layer. Therefore, the failure in the form of the observed lowering of the scour protection was presumably caused by the sinking of the entire protection into the seabed adjacent to the monopile base. However, it is interesting to discuss whether the sinking has taken place owing to the movement of filter stones into the cover layer, or movement of bed sand into the filter, or movement of sand up from between filter stones and cover stones.

Regarding the first question, whether or not sinking has taken place owing to the movement of filter stones into the cover layer, the present authors have, in Section 7.1, discussed the Terzaghi criterion in the context of the interaction between the filter layer and the cover layer, and found that the Terzaghi criterion is satisfied. This ensures that no filter stones will move into the cover layer. Furthermore, when implemented for the Horns Rev 1 conditions, the design guidelines given in Dixen *et al.* (2008) will indicate that the filter stones will not be winnowed out from between cover stones.

As for the movement of bed sand into the filter layer, or movement of sand up through both filter layer and cover layer, what happened during the period between the two surveys (see Section 1) is unknown. However, from Nielsen's (2011) physical model observations, it is likely that the sand mobilised by the horseshoe vortex inside the protection layer entrained constantly into the main body of the flow along the entire outer boundary of the horseshoe vortex ('encircling' the upstream half of the pile) until the sinking process attained a steady state, and from then on the sand deposited inside the protection layer.

Another issue is that the 50-year current speed of 0·88 m/s is too fast for normal conditions (e.g. see the synthetically generated but calibrated current time series representing current as well as tide and surge data given in Nielsen and Hansen (2007)), and therefore the normal current will lie below the critical motion trend in Figure 14 (or Figure 11). Although the data in Figure 11 were obtained from tests where the number of filter layers, N_f, is a factor of 2 larger than the Horns Rev case, the observed sinking at Horns Rev 1 can also, in part, be explained by the presence of waves in ordinary current conditions, discussed in the preceding paragraphs.

9. Conclusions

(*a*) Flow around a pile with scour protection, initiation of motion at the sediment bed beneath the scour protection, and sediment motion beneath the scour protection and resulting sinking have been described in the light of the recent work of Nielsen (2011), which is also summarised in Nielsen *et al.* (2011).

(*b*) The findings of the above work were formulated in the form of a set of non-dimensional parameters for (i) the initiation of motion beneath the scour protection, and (ii) sinking of the scour protection. The results were compared with the Horns Rev 1 case. Good agreement was obtained, with the results revealing the potential cause of failure observed from the field surveys conducted in 2002 and 2005. The latter gave confidence in the use of the results in practice.

(*c*) Scour protection has also been studied from the point of view of filter criteria, based on the work of de Graauw *et al.* (1984).

(*d*) According to the latter criteria, it was found that the filter criteria are not satisfied in the Horns Rev 1 case, consistent with the observed failure.

Acknowledgement

This study was partially funded by: (*a*) the Danish Council for Strategic Research (DSF)/Energy and Environment Programme 'Seabed Wind Farm Interaction'; (*b*) Statkraft AS (Norway) 'SOERP – Statkraft Ocean Energy Research Programme'; (*c*) DHI; (*d*) Danish GTS-universitetssamarbejde project 'Fremtidens Marine Konstruktioner'; and (*e*) EU Seventh Framework Programme 'Innovative Multi-purpose Off-shore Platforms: Planning, Design and Operation (MERMAID)'.

REFERENCES

Chiew YM (1995) Mechanics of riprap failure at bridge piers. *Journal of Hydraulic Engineering* **121(9)**: 635–643.

Chiew YM (2002) Failure mechanism of riprap layer around bridge piers. *Proceedings of the 1st International Conference on Scour of Foundations*, vol. I, pp. 70–91.

Chiew YM and Lim FH (2000) Failure behavior of riprap layer at bridge piers and live-bed conditions. *Journal of Hydraulic Engineering* **126(1)**: 43.

CIRIA/CUR/Cetmef (2007) *The Rock Manual. The Use of Rock in Hydraulic Engineering*, 2nd edn. CIRIA, London, UK, C683.

de Graauw AF, van der Meulen T and de Bye MRD (1984) Granular filters: design criteria. *Journal of Waterway, Port, Coastal and Ocean Engineering, ASCE* **110(1)**: 80–96.

de Vos L, de Rouck J, Troch P and Frigaard P (2011) Empirical design of scour protections around monopile foundations part 1: Static approach. *Coastal Engineering* **58(6)**: 540–553.

de Vos L, de Rouck J, Troch P and Frigaard P (2012) Empirical design of scour protections around monopile foundations part 2: Dynamic approach. *Coastal Engineering* **60(February)**: 286–298.

Dixen FH, Sumer BM and Fredsøe J (2008) Suction removal of sediment from between armour blocks. II. Waves. *Journal of Hydraulic Engineering, ASCE* **134(10)**: 1405–1420.

Hansen EA, Simonsen HJ, Nielsen AW, Pedersen J and Høgedal M (2007) Scour protection around offshore wind turbine foundations, full-scale measurements. *Proceedings of the European Energy Conference 2007 – EWEC 2007*, pp. 132–138.

Harris JM, Whitehouse RJS and Benson T (2010) The time evolution of scour around offshore structures. *Proceedings of the Institution of Civil Engineers – Maritime Engineering* **163(1)**: 3–17, http://dx.doi.org/10.1680/maen.2010.163.1.3.

MacCamy RC and Fuchs RA (1954) *Wave Forces on Piles: A Diffraction Theory*. U.S. Army Corps of Engineers, Beach Erosion Board, USA, Technical Memo No. 69.

Nielsen AW (2011) *Scour Protection of Offshore Wind Farms*. PhD thesis, Department of Mechanical Engineering, Technical University of Denmark, Section of Coastal, Maritime and Structural Engineering, Lyngby, Denmark.

Nielsen AW and Hansen EA (2007) Time-varying wave and current-induced scour around offshore wind turbines. *Proceedings of the International Conference on Offshore Mechanics and Arctic Engineering – OMAE*, vol. 5, pp. 399–408.

Nielsen AW, Sumer BM, Fredsøe J and Christensen ED (2011) Sinking of armour layer around a cylinder exposed to a current. *Proceedings of the Institution of Civil Engineers – Maritime Engineering* **164(4)**: 159–172, http://dx.doi.org/10.1680/maen.2011.164.4.159.

Nielsen AW, Sumer BM, Ebbe SS and Fredsøe J (2012) Experimental study on the scour around a monopile in breaking waves. *Journal of Waterway, Port, Coastal and Offshore Engineering, ASCE* **138(6)**: 501–506.

Raaijmakers TC and Rudolph D (2008a) Time-dependent scour development under combined current and waves conditions – laboratory experiments with online monitoring technique. *Proceedings of the 4th International Conference on Scour and Erosion*, vol. 1, pp. 152–161.

Raaijmakers TC and Rudolph D (2008b) Time-dependent scour development under combined current and waves conditions – hindcast of field measurements. *Proceedings of the 4th International Conference on Scour and Erosion*, vol. 1, pp. 340–347.

Raaijmakers TC, Rudolph D, Bergen MRJV and Lieshout HV (2007) Offshore windpark Egmond aan Zee – performance of scour protection and edge scour development. *Proceedings of the European Offshore Wind Conference 2007 – EOW 2007, Berlin, Germany*, p. 10.

Shields A (1936) *Application of Similarity Principles and Turbulence Research to Bedload Movement* (translated from *Anwendung der Aehnlichkeitsmechanik und der Turbulenzforschung auf die Geschiebe-bewegung, Mitteilungen der Preussischen Versuchsanstalt für Nassexbau und Schiffbau, Berlin, 1936* by Ott WP and van Uchelen JC). Soil Conservation Service Cooperative Laboratory, California Institute of Technology, Pasadena, California.

Sumer BM and Fredsøe J (1997) *Hydrodynamics Around Cylindrical Structures*, 1st edn (2nd revised edn, 2006). World Scientific, New Jersey, Singapore, London, Hong Kong.

Sumer BM and Fredsøe J (2001) Wave scour around a large vertical circular cylinder. *Journal of Waterway, Port, Coastal and Ocean Engineering, ASCE* **127(3)**: 125–134.

Sumer BM and Fredsøe J (2002) *The Mechanics of Scour in the Marine Environment*. World Scientific, New Jersey, Singapore, London and Hong Kong.

Sumer BM, Christiansen N and Fredsøe J (1997) Horseshoe vortex and vortex shedding around a vertical wall-mounted cylinder exposed to waves. *Journal of Fluid Mechanics* **332(February)**: 41–70.

Sumer BM, Dixen FH and Fredsøe J (2010) Cover stones on liquefiable soil bed under waves. *Coastal Engineering* **57(9)**: 864–873.

Sumer BM, Petersen TU, Locatelli L *et al.* (2013) Backfilling of a scour hole around a pile in waves and current. *Journal of Waterway, Port, Coastal and Offshore Engineering, ASCE* **139(1)**: 9–23.

Whitehouse RJS, Harris JM, Sutherland J and Rees J (2011a) The nature of scour development and scour protection at offshore windfarm foundations. *Marine Pollution Bulletin* **62(1)**: 73–88.

Whitehouse RJS, Sutherland J and Harris JM (2011b) Evaluating scour at marine gravity foundations. *Proceedings of the Institution of Civil Engineers – Maritime Engineering* **164(4)**: 143–157, http://dx.doi.org/10.1680/maen.2011.164.4.143.

Wittrup S (2012) Horseshoe vortex washes out the sediment around offshore wind turbines. *Ingeniøren/energi&miljø*, 16 January, see http://ing.dk/artikel/125792-hestesko-hvirvler-vasker-bunden-omkring-havvindmoeller-vaek (in Danish).